$BaMO_3$ (M=Zr, Hf, Sn) material dependence of T_c reduction in $BaMO_3$-doped $SmBa_2Cu_3O_y$ films

Akihiro Tsuruta[1], Yutaka Yoshida[1], Yusuke Ichino[1], Ataru Ichinose[2], Kaname Matsumoto[3] and Satoshi Awaji[4]

[1]Department of Energy Engineering and Science, Nagoya University, Furo-cho, Chikusa-ku, Nagoya 464-8603, Japan
[2]Electric Power Engineering Research Laboratory, Central Research Institute of Electric Power Industry, 2-6-1 Nagasaka, Yokosuka, Kanagawa 240-0196, Japan
[3]Department of Materials Science and Engineering, Kyushu Institute of Technology, 1-1 Sensui-cho, Tobata-ku, Kitakyushu 804-8550, Japan
[4]Institute for Materials Research, Tohoku University, Katahira 2-1-1, Aoba-ku, Sendai 980-8577, Japan

E-mail: tsuruta-akihiro11@ees.nagoya-u.ac.jp

Abstract. For the improvement of superconducting properties of $BaMO_3$ (M=Zr, Sn, Hf)-doped $REBa_2Cu_3O_y$ films, we focused on the T_c reduction caused by lattice misfit between $BaMO_3$ and $REBa_2Cu_3O_y$. We compared the influence on the T_c reduction of $BaZrO_3$, $BaSnO_3$ and $BaHfO_3$-doped $SmBa_2Cu_3O_y$ (SmBCO) films with various BMO contents. From the correlation between configuration of nanorods and *c*-axis expansion, it was suggested that the lattice strain working on the SmBCO matrix became stronger in the order of $BaHfO_3$, $BaZrO_3$ and $BaSnO_3$. Therefore, the combination of SmBCO and $BaHfO_3$ is better regarding the suppression of the T_c reduction compared with other combinations of SmBCO and $BaMO_3$.

1. Introduction

For the realization of the high performance superconducting applications such as superconducting magnetic energy storage (SMES) and magnetic resonance imaging (MRI) using $REBa_2Cu_3O_y$ (REBCO: RE = rare earth) coated conductors, they must have a high critical current density in the applied magnetic fields $J_c(B)$ [1]. In order to improve the in-fields J_c, it is well known that the introduction of the artificial pinning centers (APCs) is effective. So far, various kinds of APCs had been reported [2-4]. Among them, $BaMO_3$ (BMO: M = Zr, Sn, Hf) nanorods are known as strong *c*-axis correlated pinning centers in REBCO films fabricated by vapor phase epitaxial method such as a pulsed laser deposition (PLD) and a chemical vapor deposition (CVD) methods [5-8]. However, the introduction of BMO nanorods also causes a reduction of the critical temperature (T_c) in the REBCO films, because the REBCO lattice is distorted by the lattice misfit between REBCO and BMO. The *c*-axis of REBCO matrix is extended by the lattice strain and the T_c decreases. The suppression of the T_c reduction is considered to be effective for the increase in J_c of BMO-doped REBCO films. Therefore, the lattice strain in the REBCO matrix and its influence on the T_c reduction should change with the kind of BMO materials due to their different lattice constants.

In this study, we aimed to suppress the T_c reduction of the BMO-doped REBCO films such as $BaZrO_3$ (BZO), $BaSnO_3$ (BSO) and $BaHfO_3$ (BHO). We have investigated the correlations between T_c reduction and several BMO materials for BMO-doped SmBCO films with various BMO contents.

2. Experimental details

All the BMO-doped SmBCO films were deposited on $LaAlO_3$ (100) single crystalline substrates by the conventional PLD method using a KrF excimer laser (λ = 248 nm) at a repetition rate of 10 Hz. The laser energy density, distance between substrate and targets, and O_2 partial pressure during the deposition were 1.7 J/cm^2, 70 mm, and 400 mTorr, respectively. The BMO-doped SmBCO films were deposited by an alternating-targets technique (ALT-PLD) [9, 10]. We fixed substrate temperatures during the deposition of BZO-doped films (940˚C), BSO-doped films (840˚C), and BHO-doped films (960˚C). These temperatures are the optimum temperatures for the straightly growth of each BMO nanorods. We changed the BMO contents in each BMO-doped SmBCO film from 1.0 to 8.3 vol.% in order to change the nanorod density and diameter. All samples were taken O_2 post-annealing at 350˚C for 1.5 hours after the deposition. The crystalline orientation of the films was evaluated by x-ray diffraction (XRD) analysis and the microstructure of the films was investigated using high-resolution transmission electron microscope (TEM). The diameter and the number densities of nanorods were measured from the cross-sectional and plan-view TEM images. The BMO content in each film were measured by energy dispersive x-ray spectroscopy (EDX). The resistivity was measured with a physical property measurement system (PPMS: Quantum Design) by standard four-probe method. The T_c was defined from the temperature dependence of the resistivity using a resistivity criterion of 0.1 μΩ cm and the probe current was fixed to about 25 A/cm^2.

3. Results and discussion

Figure 1 (a), (b) and (c) show the cross-sectional TEM images of the 3.0 vol.% BZO-doped, 4.8 vol.% BSO-doped and 4.9 vol.% BHO-doped SmBCO films, respectively. From these TEM images, it was observed that all BMO materials formed nanorods and all nanorods grew straightly and continuously. In this study, we confirmed that nanorods grew straightly and continuously in most of all films with different BMO contents by TEM images and magnetic field angular dependence of J_c (data not shown). Therefore, it is not necessary to consider the influence of nanorods formation on the lattice strain, *c*-axis expansion and T_c reduction.

Figure 2 shows the correlation between T_c and *c*-axis length of each BMO-doped SmBCO films with various BMO contents. In all kinds of BMO-doped SmBCO films, the T_cs decreased with increasing of *c*-axis length. Additionally, these tendencies quantitatively agree for all BMO material. The correlation between T_c and *c*-axis length of the BMO-doped SmBCO films does not depend on the kind of BMO material.

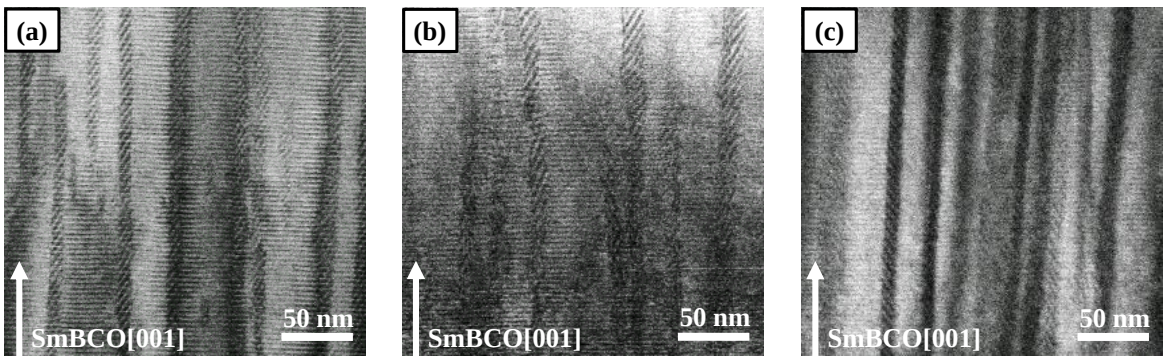

Figure 1. Cross-sectional TEM images of (a) 3.0 vol.% $BaZrO_3$-doped $SmBa_2Cu_3O_y$ film, (b) 4.8 vol.% $BaSnO_3$-doped $SmBa_2Cu_3O_y$ film, and (c) 4.9 vol.% $BaHfO_3$-doped $SmBa_2Cu_3O_y$ film.

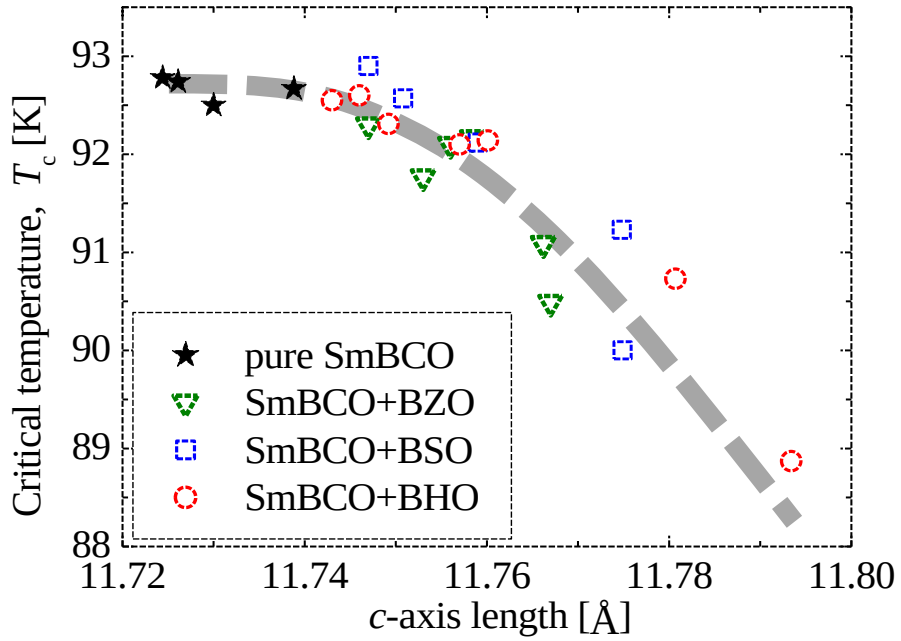

Figure 2. Correlation between T_c and *c*-axis length of each BMO-doped SmBCO film with various BMO contents.

Furthermore, we investigated the correlation between configuration of nanorods and lattice strain. Figure 3 shows the *c*-axis lengths versus the interfacial area between BMO nanorods and SmBCO matrix in unit volume and figure 4 shows the *c*-axis lengths versus the distance between adjacent nanorods interfaces. The *c*-axis length increases with increasing of interfacial area (fig. 3) or decreasing of distance between nanorods (fig. 4). In addition, the *c*-axis lengths become longer in the order of BHO-doped films, BZO-doped films and BSO-doped films at the same interfacial area or nanorods distance. From this result, it is considered that the lattice strain in the SmBCO matrix become stronger in the order of BHO, BZO and BSO. The lattice strain should be stronger with increase of lattice misfit $((3c_{BMO}-c_{SmBCO})/c_{SmBCO})$ in the order of BSO (5.4%), BHO (6.7%), and BZO (7.2%). However, these orders were different with our results. We have not clarified the reason of this difference between the order of *c*-axis expansion and lattice misfit, yet. We anticipate that the lattice strain is composed of the tensile stress by the lattice misfit and stress relaxation by the dislocations. From the results of this study, BHO might be better for the stress relaxation by the dislocations than BZO and BSO in the SmBCO matrix.

4. Conclusion

In order to suppress the T_c reduction of the BMO-doped REBCO films, we have investigated the correlations between T_c reduction and different kinds of BMO material in SmBCO films with various BMO contents. From the comparisons between T_c and *c*-axis length of each BMO-doped SmBCO film, it was revealed that the correlation between T_c and *c*-axis length is not depending on the kind of BMO material. Additionally, we investigated the correlation between configuration of nanorods and *c*-axis lengths. From the results, lattice strain became stronger in the order of BHO, BZO and BSO in both cases focusing on interfacial area and nanorods distance, and the order differed from the order of lattice misfit. In this study, it was considered that the combination of SmBCO and BHO are better for the suppression of the T_c reduction compared with other BMO-doped SmBCO films.

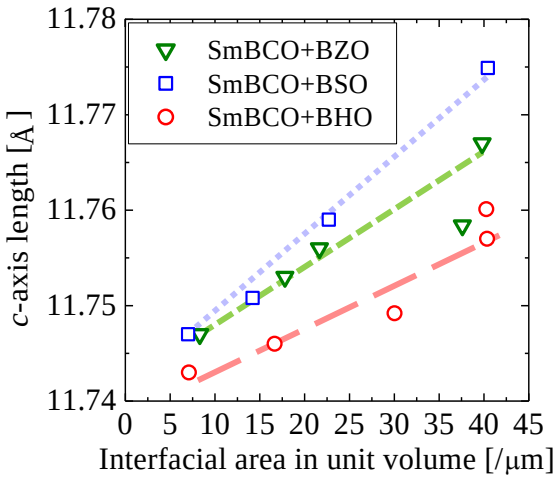

Figure 3. *C*-axis lengths versus the interfacial area between BMO nanorods and SmBCO matrix in unit volume for BMO-doped SmBCO films with various BMO contents.

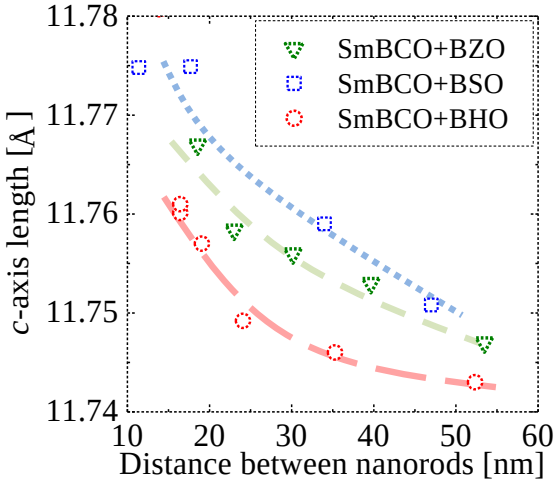

Figure 4. *C*-axis lengths versus the distance between adjacent nanorods interfaces for BMO-doped SmBCO films with various BMO contents.

Acknowledgment

This work was partly supported by Grants-in-Aid for Scientific Research (19676005, 23226014 and 25289358) and Grant-in-Aid for JSPS Fellows (25002829).

References

[1] Larbalestier D, Gurevich A, Feldmann D M and Olyanskii A 2001 *Nature* **414** 368
[2] Broussard P R, Cestone V C and Allen H R 1995 *IEEE Trans. Appl. Supercond.* **5** 1222
[3] Roas B, Hensel B, Saemann-Ischenko G and Schultz L 1989 *Appl. Phys. Lett.* **54** 1051
[4] Miura M, Kato T, Yoshizumi M, Yamada Y, Izumi T, Shiohara Y and Hirayama T 2008 *Appl. Phys. Exp.* **1** 51701
[5] Macmanus J L, Foltyn S R, Jia Q X, Wang H, Serquis A, Civale L, Maiorov B, Hawley M E, Maley M P and Peterson D E 2004 *Nature Materials* **3** 439
[6] Yamada Y, Takahashi K, Kobayashi H, Konishi M and Watanabe T et al. 2005 *Appl. Phys. Lett.* **87** 132502
[7] Mele P, Matsumoto K, Horide T, Ichinose A, Mukaida M, Yoshida Y, Horii S and Kita R 2008 *Supercond. Sci. Technol.* **21** 32002
[8] Tobita H, Notoh K, Higashikawa K, Inoue M, Kiss T, Kato T, Hirayama T, Yoshizumi M, Izumi T and Shiohara Y 2012 *Supercond. Sci. Technol.* **25** 062002
[9] Haugan T, Barnes P N, Maartense I and Cobb C B 2003 *J. Mater. Res.* **18** 2618
[10] Tsurta A, Yoshida Y, Ichino Y, Ichinose A, Matsumoto K and Awaji S 2013 *IEEE Trans. Appl. Supercond.* **23** 8001104